

## Femtosecond frequency mixing in thick bulk GaAs

Y. D. Jho, K. J. Yee, and D. S. Kim\*

*Department of Physics, Seoul National University, Seoul 151-747, Korea*

Ki-Soo Lim

*Department of Physics, Chungbuk National University, Cheongju 361-763, Korea*

(Received 25 April 2000; revised manuscript received 13 September 2000; published 6 February 2001)

Femtosecond degenerate four-wave mixing (FWM) experiments have been performed on bulk GaAs as a *continuous function of the sample thickness*. The FWM signals exhibit the transition from a real, excitonic regime to the virtual regime as the thickness increases from 3 to 17.5  $\mu\text{m}$ . The results at the negative time delay show an extraordinary signal: even when the thickness is an order of magnitude larger than the penetration depth, there still exists a signal well above the band gap. These above-the-band-gap signals are mostly confined to the negative time delay region and shift further into the negative time delay as the detection energy increases. These unusual phenomena can be understood by the third-order frequency mixing ( $2\omega_2 - \omega_1; \omega_2 > \omega_1$ ) between positively chirped spectral components.

DOI: 10.1103/PhysRevB.63.085206

PACS number(s): 78.47.+p, 78.30.Fs, 42.50.Gy, 42.65.Ky

### I. INTRODUCTION

Transient nonlinear interaction of femtosecond light pulses with semiconductors and semiconductor quantum structures has generated much interest during the past decade. Femtosecond four-wave-mixing (FWM) experiments have been intensively performed in various semiconductor structures to investigate the ultrafast nonlinear dynamics of coherent carriers.<sup>1</sup> Much research interest in those FWM studies has been focused on the excitonic properties in relatively thin samples with the thickness of the order of the penetration depth or less. On the other hand, some interesting results were obtained in moderately thick samples, including pulse propagation,<sup>2</sup> distortion,<sup>3</sup> and propagating polariton effects,<sup>4</sup> which are also dominated by exciton states. Regarding the excitation energy, most studies focused on the excitonic resonance or free carriers, while the optical Stark effect<sup>5,6</sup> and the two-photon absorption<sup>7-9</sup> utilizes intense incident light tuned to the transparent region.

For the case of excitation below the band edge, the incident light is not absorbed, thus, real carrier creation is not expected. In the two-level model approach, the carriers in this *virtual* excitation regime makes a transition from the ground state to the excited state, but can remain there for a time equal to the inverse of the detuning, consistent with the uncertainty principle. When the detuning is greater than its inhomogeneous linewidth, the creation and decay of the carriers induced by virtual transitions are determined entirely by the instantaneous exciting pulse in keeping with the adiabatic following property.<sup>5,12</sup>

Recently, strong FWM signals resulting from the below-the-exciton excitation were found in bulk semiconductors with a thickness larger than 350  $\mu\text{m}$ .<sup>10</sup> In addition, femtosecond frequency mixing in GaAs multiple quantum wells was demonstrated in femtosecond nondegenerate FWM using two synchronized, independently tunable lasers.<sup>11</sup> These previous results clearly show that the FWM signal with an off-resonant spectral component can be caused by the frequency mixing<sup>11</sup> or the instantaneously created virtual tran-

sitions in a thick sample,<sup>10</sup> and it can further originate from the free polarization decay of the off-resonant laser fields, especially in samples with large inhomogeneous broadening.<sup>13</sup> It has been reported that the below-the-exciton signals therein are present only when the two exciting pulses overlap, contrary to the resonant exciton component that survives for relatively longer time delays characterized by a dephasing time. However, there appears to be no detailed study that deals with the relative modality of the below-the-exciton and exciton signals as a continuous function of thickness. Furthermore, we note that those pulse form limited signals in the previous studies are spectrally restricted below the exciton, regardless of its generative origin.

In this paper, we have performed degenerate femtosecond FWM experiments on a wedge-like piece of GaAs, whose thickness varies between 3–17.5  $\mu\text{m}$ . The femtosecond laser spectrum is rather broad, encompassing exciton and free carrier, and extending well below the band gap. By continuously varying the sample thickness, we probe the transition from the real to a virtual regime. It is found that on the thinner side of the sample, an excitonic signal from resonantly excited real states dominates FWM. As the sample becomes thicker, a below-the-exciton signal begins to dominate. In addition, an intriguing mechanism of the FWM signal generation is found: even at the thickest end of the sample, an above-the-band-gap signal is observed. We show that this interesting signal originates from the frequency mixing of the below-the-exciton frequency components.

### II. EXPERIMENTAL DETAILS

As shown in Fig. 1(a), we have performed time-integrated (TI)-FWM and spectrum-resolved (SR)-FWM at various sample thicknesses. The bulk GaAs sample used here was lapped and polished to have the wedgelike shape with a linear thickness variation ranging from 3 to 17.5  $\mu\text{m}$  along the wedge, and the temperature was kept at 12 K. The sample thickness at each excited spot was measured by Fabry-Perot oscillations in the transmission spectrum<sup>14</sup> and the delayed

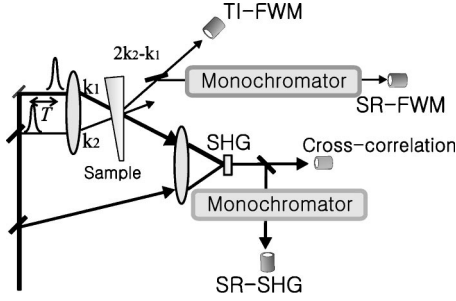


FIG. 1. Schematic of the experimental setup.  $T$ ,  $\mathbf{k}_1$ ,  $\mathbf{k}_2$ , TI-FWM, SR-FWM, SHG, and SR-SHG stand for the temporal separation between the pump and probe pulses, the pump direction, the probe direction, time-integrated four-wave mixing (FWM), spectrum resolved FWM, second-harmonic generation, and the spectrum resolved (SR) SHG, respectively.

time of a tiny secondary peak in the cross correlation (CC). CC was measured between incident and transmitted pulses using a  $200 \mu\text{m}$ -thick, phase matched,  $\beta\text{-BaB}_2\text{O}_4$  crystal. To investigate the frequency chirping caused by the linear or nonlinear dispersion during the propagation through the thick sample, the CC was spectrally divided by a monochromator in a spectrum-resolved second harmonic generation (SR-SHG) measurement at  $14.5 \mu\text{m}$ . For a reference, a FWM signal in the reflection geometry was probed as well. The excitation source used was a self-mode-locked Ti:sapphire laser with a spectral full width at half maxima (FWHM) of about  $65 \text{ meV}$ . The peak energy of the laser was tuned below

the band edge by  $28 \text{ meV}$  as can be seen in Fig. 2(a). The pump and probe pulses, with momenta  $\mathbf{k}_1$  and  $\mathbf{k}_2$  respectively, have collinear polarizations with an external crossing angle of  $5^\circ$ . Considering the pulse width of about  $30 \text{ fs}$ , the repetition rate of  $76 \text{ MHz}$ , and the focused spot size of about  $100 \mu\text{m}$ , the pump intensity is estimated to be about  $200 \text{ MW/cm}^2$  per pulse; probe intensity was kept a third of that of the pump.

### III. EXPERIMENTAL RESULTS AND DISCUSSIONS

#### A. SR-FWM as a function of sample thickness

Though the off-resonant and on-resonant FWM signals show different temporal behaviors, we have both signals during the overlap of the excitation laser pulses. At this zero delay time, therefore, we can estimate the thickness dependence of the off-resonant and on-resonant FWM signals. If we exclude absorption and assume that the area of spatial and temporal overlap between two pulses does not change significantly through the thickness variation, the signal intensities are expected to increase quadratically with sample thickness since the amplitude of the macroscopic polarization is linearly proportional to the interaction volume. Hence, SR-FWM signals induced by virtual transitions as a function of thickness can be given by

$$I_{\text{virtual}}(E, l) \propto l^2, \quad (3.1)$$

where  $E$  is an energy below the band gap where little or no absorption occurs. Now, for the above-the-band-gap real excitations, including only absorption and neglecting other complicating effects caused by relatively high laser intensity with wide spectrum and long propagation distance, the SR-FWM intensity from the on-resonant excitation can be simplified as

$$\begin{aligned} I_{\text{real}}(E, l) &\propto |\mathbf{E}_{2\mathbf{k}_2 - \mathbf{k}_1}|^2 \propto \left| \int_0^l (\mathbf{E}_0 e^{-\alpha z/2})^3 dz e^{-\alpha(l-z)/2z} \right|^2 \\ &= \left| \mathbf{E}_0^3 e^{-\alpha l/2} \left( \frac{1 - e^{-\alpha l}}{\alpha} \right) \right|^2 \\ &= I_0^3 e^{-\alpha(E)l} \left( \frac{1 - e^{-\alpha l}}{\alpha} \right)^2, \end{aligned} \quad (3.2)$$

where  $\alpha(E)$ ,  $\mathbf{E}_0$ , and  $\mathbf{E}_{2\mathbf{k}_2 - \mathbf{k}_1}$  are, respectively, the absorption coefficient at energy  $E$ , the amplitude of the incident electric field for the incident excitation intensity  $I_0$ , and the electric field of the transmitted FWM signal in the phase-matched direction  $2\mathbf{k}_2 - \mathbf{k}_1$ . As a function of  $l$ , Eq. (3.2) increases at first and then decreases exponentially. We notice that Eq. (3.2) converges to Eq. (3.1) as  $\alpha$  approaches to zero.

Figure 2(a) shows the excitation laser spectrum (dotted line) and absorption coefficient (solid line). FWM signals, as a function of thickness, are plotted at zero time delay in Fig. 2(b) for a below-the-band-gap detection energy (at  $1.485 \text{ eV}$ ) and Fig. 2(c) for a detection energy at the exciton resonance (at  $1.514 \text{ eV}$ ). The detection energy was fixed using a monochromator and the thickness was continuously varied. At the below-the-band-gap energy, the *virtual* FWM signal in-

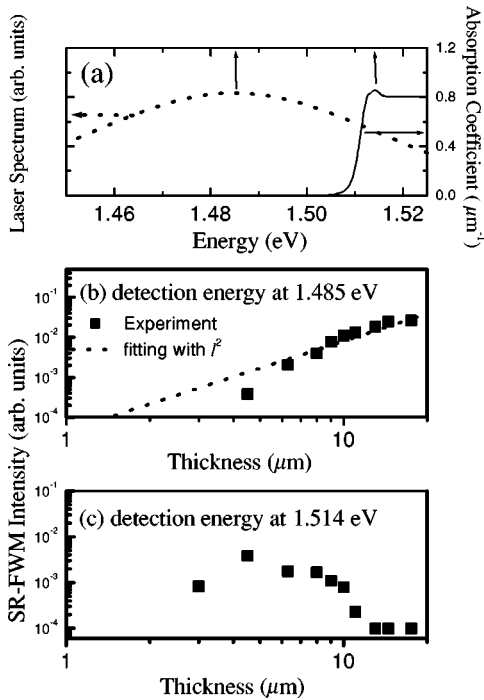


FIG. 2. (a) Laser spectrum (dotted line) and the absorption coefficient (solid line). (b) SR-FWM signals measured at the exciton energy (at  $1.514 \text{ eV}$ ) and (c) at the laser center energy (at  $1.485 \text{ eV}$ ), as a function of the sample thickness. The spectral position corresponding to (b) and (c) is denoted by vertical arrows in (a).

increases nearly quadratically with the sample thickness, as shown in Fig. 2(b). This is in good agreement with Eq. (3.1). Near the excitonic peak, as shown in Fig. 2(c), the signal at first increases and then decreases, in good qualitative agreement with Eq. (3.2), although it is clear that such simple estimations are too crude to accurately explain the signal traces.

As the off-resonantly excited signals are in the adiabatic following limit, the noninteracting two-level model can be suitable.<sup>12</sup> In the non-interacting two-level model approach, the SR-FWM signal shows the Lorentzian line shape:  $1/[(\Gamma/2)^2 + \Delta^2]$ , where  $\Delta$  is the detuning from exciton energy and  $\Gamma$  is the exciton linewidth (FWHM) including a power-broadened factor. To estimate the SR-FWM as a function of thickness over all the spectral range, we summed the real and the virtual part assuming that they are both in the shape of the Lorentzian. Because the quantitative calculation of the real and virtual transition strengths is extremely difficult in this thick sample, the experimental values of  $I_{real}(E_x, l)$  (measured at 1.514 eV) and  $I_{virtual}(E_L, l)$  (measured at 1.485 eV), as given in Fig. 2(b) and Fig. 2(c), were incorporated into the fitting form, representing the real and virtual part of the signal, respectively. Therefore, the simplified *phenomenological* fitting form of the signal intensity from the two competing contributions of the on-resonant and off-resonant components at various thickness is

$$\begin{aligned}
 I(E, l) &= I_{real}(E, l) + I_{virtual}(E, l) \\
 &= I_{real}(E_x, l) \left[ \frac{I_{real}(E, l)}{I_{real}(E_x, l)} \right] \\
 &\quad + I_{virtual}(E_L, l) \left[ \frac{I_{virtual}(E, l)}{I_{virtual}(E_L, l)} \right] \\
 &\approx I_{real}(E_x, l) \frac{(\Gamma/2)^2}{[(\Gamma/2)^2 + \Delta^2]} e^{[\alpha(E_x) - \alpha(E)] \cdot l} \\
 &\quad + I_{virtual}(E_L, l) \frac{[(\Gamma/2)^2 + (E_L - E_x)^2]}{[(\Gamma/2)^2 + \Delta^2]} \\
 &\quad \times \left[ \frac{I_0(E) e^{-\alpha(E) \cdot l}}{I_0(E_L)} \right]^3, \tag{3.3}
 \end{aligned}$$

where  $I_{real}(E, l)$  and  $I_{virtual}(E, l)$  represent the FWM signal induced by on-resonant and off-resonant transitions, respectively.  $E_L$  corresponds to the center energy of the incident laser spectrum  $I_0(E)$ . The off-resonant FWM signal is assumed to be cubically proportional to the transmitted laser spectrum at the sample thickness  $l$ :  $I_{virtual}(E, l) \propto [I_0(E) \cdot e^{-\alpha(E) \cdot l}]^3$  in the last term, because it is affected by the laser intensity over all the broad spectral range, in contrast to the on-resonant signal whose energy mostly corresponds to the lowest exciton resonance.

Figure 3 shows SR-FWM at zero time delay for various sample thicknesses. Solid lines and dotted lines correspond to the experimental data and the fitting based on Eq. (3.3), respectively.  $\Gamma$  of 8.4 meV was measured in reflective FWM for our excitation condition to be used for the fitting. Each trace is normalized to have the same maximum value. The fitting curves and the experimental data are in good agree-

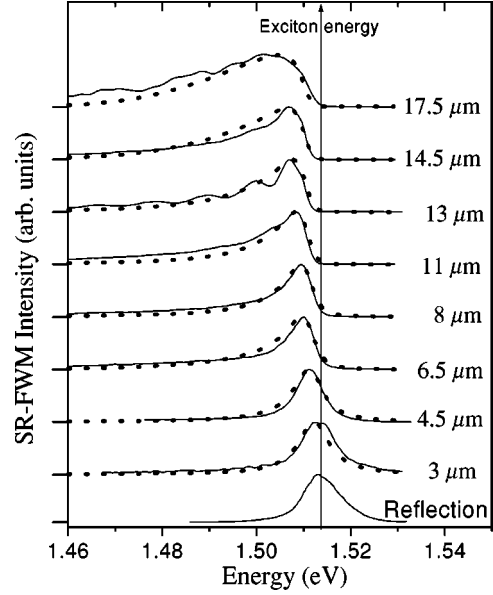


FIG. 3. The measured SR-FWM signals (solid lines) at zero time delay, at various sample thicknesses from 3 to 17.5  $\mu\text{m}$ . The Lorentzian-shape fitting curves using the measured real and virtual signals in Fig. 2(b) and 2(c) for each thickness are shown with dotted lines. The bottom trace corresponds to the reflective SR-FWM signal.

ment, revealing the obvious spectrum shift from an exciton-dominant real regime to a virtual regime whose energy is below the band edge, as the thickness increases from 3 to 17.5  $\mu\text{m}$ . While the excitonic signal decreases exponentially with increasing sample thickness, the virtual signal keeps increasing with the sample thickness. As a result, at about 10  $\mu\text{m}$  of sample thickness, the signal at the excitonic energy or above is nearly all gone. Note that the oscillatory behavior observed at 13  $\mu\text{m}$  is caused by the Fabry-Perot resonance.<sup>14</sup>

## B. Frequency mixing

Any excitonic FWM signal created at the input end of the sample would have been long vanished due to the absorption during propagating through the sample that is much larger than the penetration depth, and likewise, the incident spectral component whose energy is larger than the exciton. In Fig. 4, a logarithmic plot of both the transmitted laser intensity (top) and SR-FWM signal at the zero time delay (bottom, dotted line) actually shows the *excitonic dip* for the sample thickness of 14.5  $\mu\text{m}$ . This clearly shows why the signal at or above the excitonic resonance disappears for thick samples: it is due to simple absorption of both the signal and the laser. To our surprise, however, we found that as the delay time becomes negative (bottom, solid line), above-the-exciton FWM signals become stronger, by more than two orders of magnitudes. This is unexpected, for the penetration depth near the band edge of GaAs is only about 1  $\mu\text{m}$ , so that any excitonic and above-the-band-gap signal is expected to be completely attenuated at this thickness. Note, on the other hand, that the below-the-band-gap signals are smaller at this time delay compared with those at zero delay.

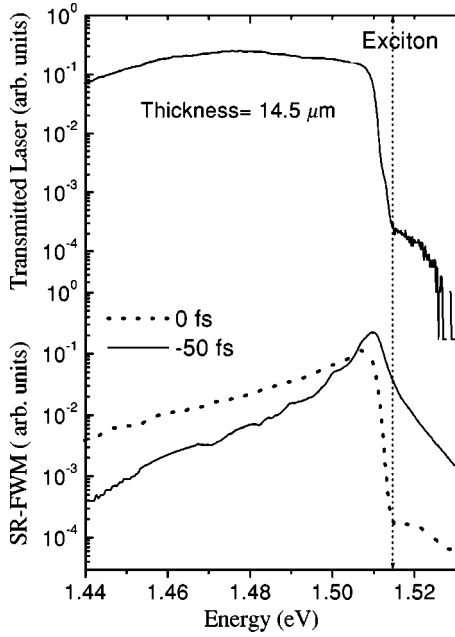


FIG. 4. Transmitted laser (top, solid line) and SR-FWM at 0 fs (bottom, dotted line) and  $-50$  fs (bottom, solid line). The vertical line denotes the excitonic peak and the sample thickness is  $14.5 \mu\text{m}$ .

To comprehend the generation mechanism of the absorbable signal seemingly transmitted through the enormous thickness, we have measured the *spectrally resolved* (SR)-TI-FWM as shown in Fig. 5. Figure 5 shows temporal shapes of SR-TI-FWM signals transmitted through relatively thick [ $14.5 \mu\text{m}$ ; (a)] or thin [ $4.5 \mu\text{m}$ ; (b)] sample positions. The detection energies  $E_D (\equiv E_x + \Delta_D)$  in meV scale were fixed at the values denoted in the figure window for each TI-FWM measurement. All signals are normalized to have the same maximum value. For the energy far below the exciton, the signal peaks more or less at the zero delay. On the contrary,

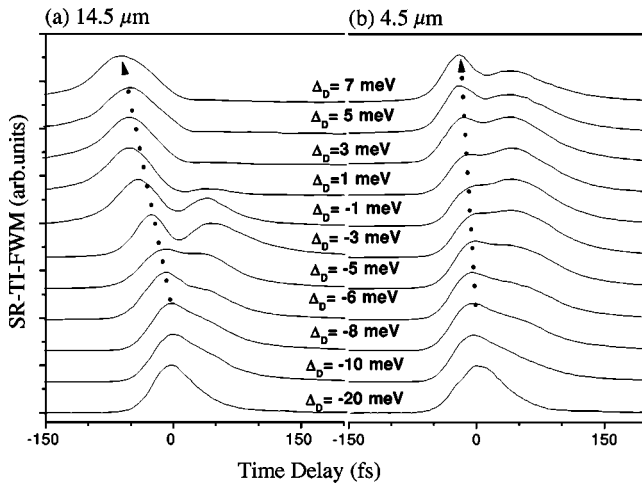


FIG. 5. Spectrum resolved (SR)-TI-FWM at various detection energies.  $\Delta_D$  is the energy above exciton in meV scale. The thickness is  $14.5 \mu\text{m}$  for (a) and  $4.5 \mu\text{m}$  for (b). The dotted arrows are along the time delays at which FWM signals peak for the first time.

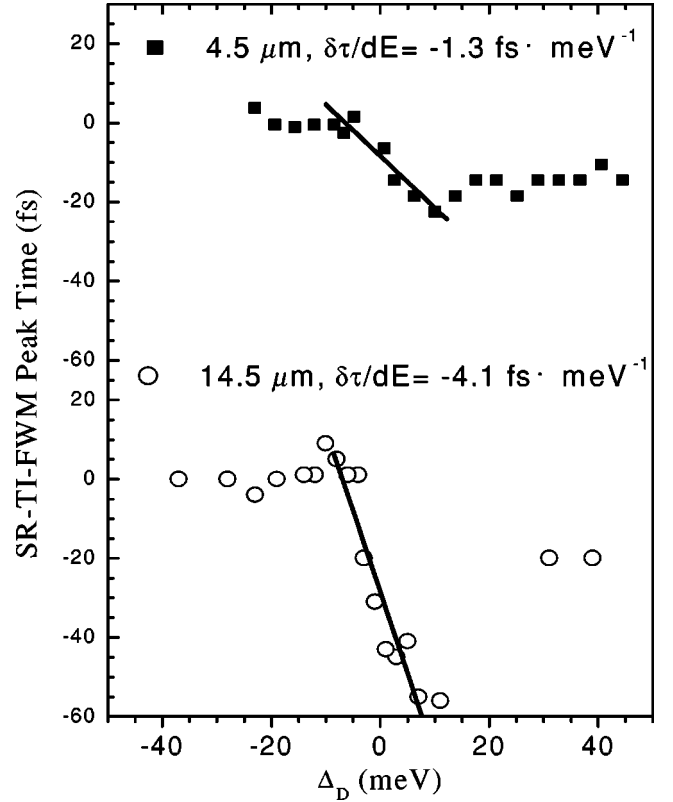


FIG. 6. Times at which the first SR-TI-FWM peak appear for  $4.5 \mu\text{m}$  (top, solid square) and  $14.5 \mu\text{m}$  (bottom, open circle) over broad detection energy. Solid lines are the linear fit of data in the region that shows the linear shift at each thickness.

the higher the energy of the above-the-band-gap signals is, the larger the negative time delay value at which this component peaks is (see the dotted arrow). Note that the shift toward the negative time delay with increasing detection energy is more drastic for the thickness of  $14.5 \mu\text{m}$  than for  $4.5 \mu\text{m}$ . This suggests that there might be a role played by the group velocity dispersion; the FWM signals are made after the excitation laser propagate through the sample to a certain degree.

To see the temporal shift of signals with detection energy more clearly, we have plotted the peak-time  $\tau$  as a function of detection energy  $\Delta_D$  in Fig. 6 over a broad range of detection energy. In Fig. 6, the slope  $d\tau/d\Delta_D$  was linearly fitted with a constant  $-4.1 \text{ fs/meV}$  for  $14.5 \mu\text{m}$  and  $-1.3 \text{ fs/meV}$  for  $4.5 \mu\text{m}$  in the near-exciton region. We note that (1) the ratio of these slopes agrees well with that of their thicknesses. (2) The presence of the signals at the negative time delays and peak time shift is limited only to the so-called real regime in which the linear absorption is meaningful, in spite of the broad range of detection energies. (3) After  $\tau$  approaches the limit of pulse duration time ( $\sim 74 \text{ fs}$  for  $14.5 \mu\text{m}$  and  $\sim 45 \text{ fs}$  for  $4.5 \mu\text{m}$ ), it stays constant near  $-20 \text{ fs}$  even with increasing detection energy, which is slightly shorter than the incident pulse width. All the above-mentioned phenomena can be adequately understood if we assume that the above-the-exciton FWM signal is coming from the third order frequency mixing ( $2\omega_2$

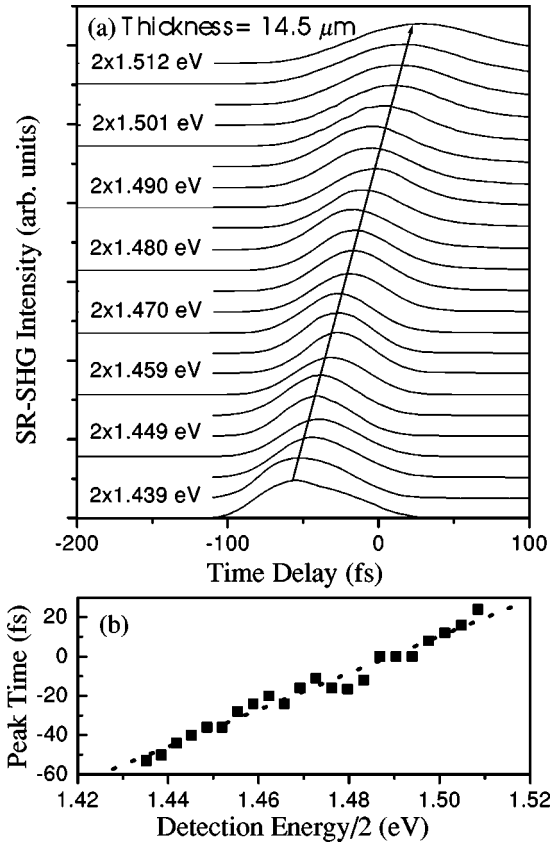


FIG. 7. (a) SR-SHG intensity at  $14.5 \mu\text{m}$  for each fixed energy that is denoted in the figure. (b) Peak times of the SR-SHG signals as a function of half the detection energy (solid square) and the linear fitting curve (dotted line).

$-\omega_1; \omega_2 > \omega_1$ ) mostly at the back side of the sample. The two frequency components  $\omega_2$  and  $\omega_1$  can be any two frequency components of the broad femtosecond laser spectrum. The fact that it is indeed coming from the back side is supported by the fact that the above-the-exciton signals exist predominantly at the negative time delay, which indicates that the mixing was done after propagating to some extent through the sample, undergoing positive chirping. As a contrapositive example, if the above-the-exciton FWM signals had been made near the incident surface, they should have been absorbed during propagation.

The positive chirping has indeed been observed in Fig. 7. Figure 7 (a) shows the results of spectrum-resolved second harmonic generation correlation (SR-SHG)<sup>15</sup> between incident pulse and transmitted pulse measured at sample thickness  $14.5 \mu\text{m}$ . In this measurement, the SHG output is spectrally resolved by a monochromator, and the time-averaged intensity of this spectrum-resolved second harmonic light is measured as a function of both the frequency in the second harmonic region and the delay time between the two input pulses. In Fig. 7(a), we see that each below-the-band-edge frequency travels at a slightly different speed and the SR-SHG are temporally broader than the input pulse with FWHM of 30 fs. The traces near the exciton were especially broad. The delayed peak time shows a monotonic linearity, which indicates the pump-induced nonlinear dispersion can

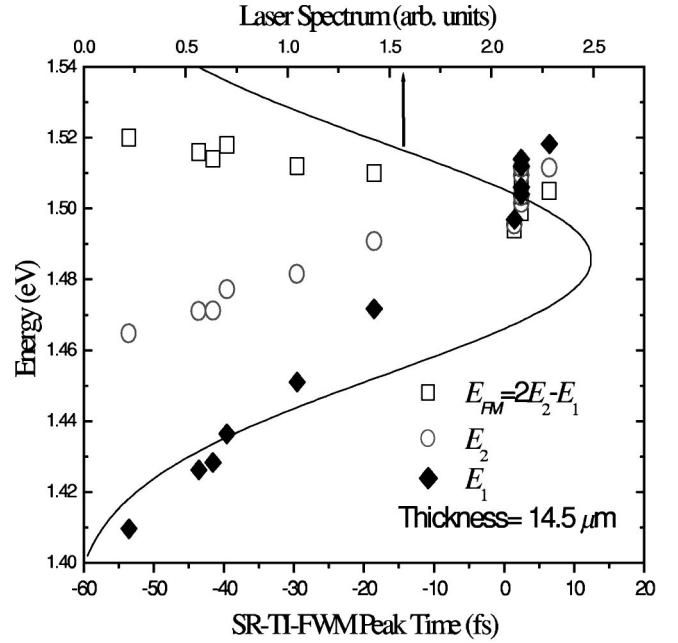


FIG. 8. Estimated mixing components  $E_2$  (open circle) and  $E_1$  (solid diamond) for the results along the dotted arrow in Fig. 5(a), induced from group-delay dispersion and the detected energy  $E_{FM}(\tau)$  (open square). The solid line is the laser spectrum.

be neglected for our intensity and thickness. Lower frequencies travel ahead of higher frequencies, indicating a positive chirping. The group-delay dispersion (GDD) as shown in Fig. 7(a) is fitted well with the slope  $dt(E)/dE = 0.97 \text{ fs/meV}$  as in Fig. 7(b), where  $t(E)$  is the time where the SR-SHG signal with energy  $2E$  peaks.

If the two off-resonant spectral components of probe pulse ( $E_2 = \hbar\omega_2$ ) and pump pulse ( $E_1 = \hbar\omega_1$ ) with  $E_2 > E_1$  undergo the GDD during propagation due to the positive chirping, the time delay has to be negative for the two components to temporally meet and mix near the exit end of the sample. Therefore, the higher the detection energy ( $= 2E_2 - E_1$ ) is, the larger the difference between mixing energies should be, and, the larger the negative time delay at which it peaks. This is consistent with our observation, shown in Figs. 5 and 6. In principle, one should consider the frequency mixing in every depth of the sample, and therefore, include the different absorption and dispersion before and after the frequency mixing, which will show various contributions in time and spectral domain. However, if the sample thickness is much larger than the penetration depth, the frequency mixing signals made other than at the exit end can be neglected in the absorbable spectral range. On the other hand, when the energy of the frequency mixing signal is below the absorption edge, the signal is not necessarily made only at the exit end, but it is possible for it to be produced anywhere between the incident surface and the exit-end of the sample. Below-the-band edge signals also can be made between various spectral components of the excitation laser. Nevertheless, the energies of the mixing components should be the same for the temporal overlap between the two pulses to be preserved all though the propagation, i.e., for the two pulses not to be dispersed. Therefore, the frequency mixing signals

far below the exciton energy are at the peak of their intensities near the zero time delay, without showing any notable temporal shift with the detection energy change. In addition, the large sample thickness produces more signal because of larger interaction volume, while it prohibits an otherwise more efficient frequency mixing involving on-resonant spectrum. At present, we do not understand why for larger  $\Delta_D$ , the peak time delay stays the same (at 4.5  $\mu\text{m}$ ) or even gets smaller (at 14.5  $\mu\text{m}$ ).

In our model, for a given above-the-exciton detection energy, we can easily find the two main frequency components  $E_2 (= \hbar\omega_2$  for probe) and  $E_1 (= \hbar\omega_1$  for pump) that mix. Since the resulting frequency mixing energy  $E_{FM}$  satisfies the relation:

$$\begin{aligned} E_{FM}(\tau) - E_2(t_2) &= E_2(t_2) - E_1(t_1) \\ &= \int_{t_1}^{t_2} (\delta E / \delta t) dt \approx (t_2 - t_1) / 0.97 \text{ meV/fs}, \end{aligned} \quad (3.4)$$

we can calculate  $E_2$  and  $E_1$  for a given  $E_{FM}$  when  $(t_2 - t_1)$  is determined, where  $t_2(t_1)$  is the time that the spectral component with energy  $E_2(E_1)$  spends during propagation through the sample before it is mixed with  $E_1(E_2)$ . Note that the value 0.97 meV/fs was obtained for the sample thickness 14.5  $\mu\text{m}$  from Fig. 7. The temporal difference  $-(t_2 - t_1)$  corresponds to the suitable time delay for the two frequency components to meet at the back side of the sample and is approximately the same with  $\tau$  in the context of frequency mixing.  $\delta E / \delta t$  was assumed to be a constant obtained through SR-SHG measurement. In Fig. 8, we estimate the

mixing components along the dotted arrow of Fig. 5 (a) by using Eq. (3.4). As shown in Fig. 8, even with these drastic approximations, both  $E_1$  (open circle) and  $E_2$  (solid diamond) fall approximately in the lower energy side of the incident laser spectrum (solid line), which largely survives the propagation through the sample. This further supports our interpretation that the above-the-gap signal originates from the combined effect of linear group velocity dispersion and third-order frequency mixing.

#### IV. CONCLUSION

In conclusion, we performed degenerate FWM measurements on a wedgelike GaAs bulk sample whose thickness varies continuously across the sample. Over the thickness range, we observed the clear spectral trace associated with the resonantly excited exciton signals and the nonresonantly created signals in the virtual states. In addition, an above-the-band-gap signal that survives seemingly the enormous sample thickness is found and is explained by the frequency mixing near the exit end of the thick sample, combined with the linear chirping. It is common sense that above-the-band gap signals cannot survive propagation through optically very thick samples. Our experiments show a nature's ingenious way of overriding this restriction.

#### ACKNOWLEDGMENTS

This work was supported by MOST (the National Research Laboratory Program and the Nanostructure Technology Project) and KOSEF (the Center for Strongly Correlated Materials Research, and Grant No. 97-0702-03-01-3).

\*Corresponding author. Email: denny@phya.snu.ac.kr

<sup>1</sup>J. Shah, *Ultrafast Spectroscopy of Semiconductors and Semiconductor Nanostructures*, Vol. 115 (Springer-Verlag, Berlin, 1996), and references therein.

<sup>2</sup>R. G. Ulbrich and G. W. Fehrenbach, *Phys. Rev. Lett.* **43**, 963 (1979).

<sup>3</sup>D. S. Kim, J. Shah, D. A. B. Miller, T. C. Damen, W. Schäfer, and L. N. Pfeiffer, *Phys. Rev. B* **48**, 17 902 (1993).

<sup>4</sup>T. Rappen, G. Mohs, and M. Wegener, *Phys. Rev. B* **47**, 9658 (1993); K.-H. Pantke, P. Schillak, B. S. Razbirin, V. G. Lysenko, and J. M. Hvam, *Phys. Rev. Lett.* **70**, 327 (1993).

<sup>5</sup>A. Mysyrowicz, D. Hulin, A. Antonetti, A. Migus, W. T. Masselink, and H. Morkoc, *Phys. Rev. Lett.* **56**, 2748 (1986); S. Schmitt-Rink and D. S. Chemla, *ibid.* **57**, 2752 (1986); S. G. Lee, P. Harten, J. P. Sokoloff, R. Jin, B. Fluegel, K. E. Meissner, C. L. Chuang, R. Binder, S. W. Koch, G. Khitrova, H. M. Gibbs, N. Peyghambarian, J. N. Polky, and G. A. Pubanz, *Phys. Rev. B* **43**, 1719 (1991).

<sup>6</sup>M. Yamanishi, *Phys. Rev. Lett.* **59**, 1014 (1987); D. S. Chemla, D. A. B. Miller, and S. Schmitt-Rink, *ibid.* **59**, 1018 (1987).

<sup>7</sup>J.-F. Lami and C. Hirlimann, *Phys. Rev. B* **60**, 4763 (1999).

<sup>8</sup>C.-K. Sun, J.-C. Liang, J.-C. Wang, F.-J. Kao, S. Keller, M. P.

Mack, U. Mishra, and S. P. DenBarrs, *Appl. Phys. Lett.* **76**, 439 (2000); D. Kim, I. H. Libon, C. Voelkmann, Y. R. Shen, and V. Petrova-Koch, *Phys. Rev. B* **55**, R4907 (1997).

<sup>9</sup>J. S. Yahng, D. S. Kim, N. Del. Fatti, and F. Vallée, *J. Opt. Soc. Kor.* **1**, 100 (1997).

<sup>10</sup>S. Yu, J. H. Chu, J. I. Lee, D. Kim, Y. H. Yee, D. S. Kim, J.-Y. Leem, C.-R. Lee, and J. H. Lee, *Appl. Phys. Lett.* **69**, 79 (1996); S. Yu, D. Kim, D. S. Kim, Y. H. Lee, Y. H. Cho, and B. D. Choe, and J. H. Lee, *J. Appl. Phys.* **81**, 6928 (1997); Sung Kyu Yu, Joo In Lee, Dong Ho Kim, D. S. Kim, and Jong Hyun Lee, *J. Korean Phys. Soc.* **30**, 391 (1997).

<sup>11</sup>Y. H. Ahn, J. S. Yahng, J. Y. Sohn, K. J. Yee, S. C. Hohng, J. C. Woo, D. S. Kim, T. Meier, S. W. Koch, Y. S. Lim, and E. K. Kim, *Phys. Rev. Lett.* **82**, 3879 (1999).

<sup>12</sup>M. D. Crisp, *Phys. Rev. A* **8**, 2128 (1973).

<sup>13</sup>D. S. Kim, J. Shah, T. C. Damen, W. Schäfer, L. N. Pfeiffer, and K. Kähler, *Phys. Rev. B* **50**, 15 086 (1994).

<sup>14</sup>M. I. Nathan, A. B. Fowler, and G. Burns, *Phys. Rev. Lett.* **11**, 152 (1963).

<sup>15</sup>Y. Ishida, K. Nakanuma, and T. Yajima, *IEEE J. Quantum Electron.* **21**, 69 (1988).